Monte Carlo study of the superspin glass behavior of interacting ultrasmall ferrimagnetic nanoparticles

M. Vasilakaki,[1] G. Margaris,[1] D. Peddis,[2] R. Mathieu,[3] N. Yaacoub,[4] D. Fiorani,[2,5] and K. Trohidou[1,*]

[1]*Institute of Nanoscience and Nanotechnology, NCSR "Demokritos," 153 10 Aghia Paraskevi, Attiki, Greece*

[2]*Istituto di Struttura della Materia-CNR, 00015 Monterotondo Scalo (RM), Italy*

[3]*Department of Engineering Sciences, Uppsala University, Box 534, SE-751 21 Uppsala, Sweden*

[4]*LUNAM, Université du Maine, Institut des Molécules et Matériaux du Mans CNRS UMR-6283, F-72085 Le Mans, France*

[5]*Center of Nanomaterials Research, Immanuel Kant Baltic Federal University, Kaliningrad, Russia*

(Received 18 October 2017; revised manuscript received 5 February 2018; published 14 March 2018)

The magnetism of a dense assembly of ultrasmall ferrimagnetic nanoparticles exhibits unique features due to the combination of intraparticle and strong interparticle interactions. To model such system we need to account for the internal particle structure and the short- and long-range interparticle interactions. We have developed a mesoscopic model for the particle assembly that includes three spins (two for the surface and one for the core) for the description of each nanoparticle, interparticle dipolar interactions and the interparticle exchange interactions for the nanoparticles in contact. The temperature dependence of the observed exchange bias effect, due to exchange coupling at the interface between core/surface spins and the interparticle exchange coupling, and the zero-field-cooled–field-cooled magnetization vs temperature curves have been investigated using the Monte Carlo simulation technique with the implementation of the Metropolis algorithm. Our simulations reproduce well the experimental data of ultrasmall ∼2-nm $MnFe_2O_4$ nanoparticles, confirming the close relationship between the superspin glass state and the exchange-bias effect in dense nanoparticle systems, owing to the interplay between the intraparticle structure and the interparticle effects.

DOI: 10.1103/PhysRevB.97.094413

I. INTRODUCTION

Magnetic nanoparticles have attracted much interest thanks to their technological [1] and biomedical applications [2]. The advances in the synthesis methods have allowed the production of very small particles. The reduction of their size at nanoscale leads to the appearance of finite-size and -surface effects that provide to the nanoparticles unique characteristics and magnetic properties. The reduced symmetry of surface atoms due to broken exchange bonds results in high anisotropy, frustration, and spin disorder at surface. As a consequence, single-domain magnetic nanoparticles consist usually of a magnetically ordered (or quasiordered for ultrasmall particles) core surrounded by a magnetically disordered surface where the spins are randomly oriented [3–8]. In addition, as the size decreases the surface-to volume-ratio increases and the surface layer properties dominate the magnetic properties of particles. This effect is particularly important for antiferromagnetic and ferrimagnetic particles.

Alves *et al.* [9] found that $MnFe_2O_4$ nanoparticles of average size 3.3 and 7 nm have effective anisotropy constant values of 8.7×10^6 and 2×10^6 erg/cm^3, respectively, i.e. two orders of magnitude larger than the first-order magnetocrystalline anisotropy constant of bulk $MnFe_2O_4$ equal to 3×10^4 erg/cm^3. These differences are due to the increased surface anisotropy with decreasing particle size. Moreover, the interface exchange coupling between particle core and surface is responsible for the exchange-bias effect [8].

The presence of interparticle interactions, namely the dipole-dipole interactions between nanoparticles and the exchange interactions occurring between the magnetic spins at the surface of neighboring particles in contact, plays a key role on the magnetic behavior of particle assemblies [10,11]. In dense nanoparticle systems such interactions among randomly oriented particle moments can lead to a collective disordered magnetic state of superspin glass (SSG) type [12]. The interplay with particle-size effects can give rise to unique properties. Spinel ferrites nanoparticles [13–16] are particularly attractive in this context as they provide a further tool to tune the anisotropy and particle moment through the control, by means of the size, composition, and preparation method, of the cation distribution between the tetrahedral and octahedral sublattices of the spinel structure. The magnetic properties of such materials are of interest in data storage and ferrofluid technology.

Experiments on assemblies of coated $MnFe_2O_4$ of around 7–8 nm showed that they behave as weakly interacting systems [17,18] but their powders exhibit strong interparticle interactions [19], leading to collective superspin glass systems for very small diameters [20,21]. Therefore the magnetic behavior of the above systems depends on the single-particle characteristics, the interparticle interactions, and their interplay. Detailed experimental and theoretical investigations are necessary to understand the above effects.

Modeling assemblies of nanoparticles with core/surface morphology become a very complicated issue. In this case, the model has to take into account, together with the interparticle interactions, the intraparticle characteristics. In this work we have developed a simple mesoscopic model to simulate the magnetic properties of assemblies of ultrasmall ferrimagnetic

*Corresponding author: k.trohidou@inn.demokritos.gr

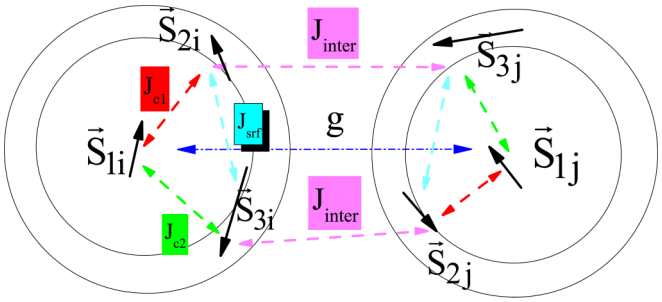

FIG. 1. Schematic representation of the spin structure of a pair of nanoparticles and the intra- and interparticle interactions.

nanoparticles with core/surface morphology. Our mesoscopic model is based on the reduction of the amount of simulated spins to the minimum number necessary to describe the magnetic structure of the core/surface particles and on the introduction of the adequate exchange and anisotropy parameters between the different spin regions inside the nanoparticle. Our modeling is multiscaled since the magnetic moments are evaluated using data from our atomistic simulations of the core/surface nanoparticles. Then we integrate them properly into the mesoscopic model going in this way from the atomic scale to the mesoscopic scale modeling. Our mesoscopic model for nanoparticle assemblies with a core/shell morphology has already been proved to be a useful and effective tool to predict and explain the experimentally observed exchange-bias properties of bimagnetic core/shell nanoparticle assemblies as Co/CoO nanoparticles [22].

In the present work we study the magnetic behavior of a dense assembly of ultrasmall ferrimagnetic nanoparticles. We describe each nanoparticle with a core/surface morphology considering three randomly oriented spins, one for the ferrimagnetic core and two for the two sublattices of the ferrimagnetic surface with strong random surface anisotropy as it is suggested by Rietveld refinement (a detailed description of Rietveld refinement of this sample is reported in Ref. [23])and Mössbauer spectra under magnetic fields (Supplemental Material, Ref. [24]) for ultrasmall $MnFe_2O_4$ nanoparticles of $\sim$2.0 nm. Our model, including surface effects, intraparticle and interparticle interactions, describes well the observed magnetic behavior of a superspin glass system of $MnFe_2O_4$ nanopowders.

In what follows we first describe the mesoscopic model that we have developed for the description of the dense assembly and we discuss the related parameters we have introduced in the model. Then we present our results for the temperature-dependent magnetization and the hysteresis loops and we discuss the effect of the intraparticle and interparticle characteristics on the magnetic behavior of these assemblies. In all the cases a comparison is given with the experimental measurements on $MnFe_2O_4$ nanopowders.

II. MODEL

We consider a dense assembly (concentration $p = 50\%$) of N spherical ferrimagnetic nanoparticles with core/surface morphology, located randomly on the nodes of a cubic lattice inside a box of $10\alpha \times 10\alpha \times 10\alpha$, where α is the smallest interparticle distance. Each nanoparticle is described by a set of three classical spin vectors one for the core $\vec{s}_{1i} = s_{x1i} + s_{y1i} + s_{z1i}$ and two for the surface $\vec{s}_{2i} = s_{x2i} + s_{y2i} + s_{z2i}$ and $\vec{s}_{3i} = s_{x3i} + s_{y3i} + s_{z3i}$ with magnetic moment $\vec{m}_{n,i} = m_n \vec{s}_{n,i}$, where $m_n = M_n V_n / M_s V$, $i = 1, \ldots, N$ (total number of particles), $n = 1$ stands for the core, and $n = 2,3$ for the "up" and "down" surface sublattices of the nanoparticle, respectively (Fig. 1). V is the particle volume and M_S its saturation magnetization. V_n and M_n are the volume and the saturation magnetization of the core, the up and the down surface sublattices spins.

Each spin has a uniaxial easy anisotropy axis randomly oriented. Short-range intraparticle exchange interaction between the core spin with each of the two surface spin (interface coupling J_{c1} and J_{c2}) and between the two surface spin (surface coupling $J_{\rm srf}$) are introduced as well as interparticle dipolar interactions and exchange interactions between particles in the case they are in contact, $J_{\rm inter}$.

The total energy of the system for the N nanoparticles is

$$E = -\frac{1}{2}\sum_{i=1}^{N}[J_{c1}(\vec{s}_{1i}\cdot\vec{s}_{2i}) + J_{c2}(\vec{s}_{1i}\cdot\vec{s}_{3i}) + J_{\rm srf}(\vec{s}_{2i}\cdot\vec{s}_{3i})] - \sum_{i=1}^{N} K_c V_1 (\vec{s}_{1i}\cdot\hat{e}_{1i})^2 - \sum_{i=1}^{N} K_{\rm srf}[V_2(\vec{s}_{2i}\cdot\hat{e}_{2i})^2 + V_3(\vec{s}_{3i}\cdot\hat{e}_{3i})^2]$$
$$-\frac{1}{2}g\sum_{\substack{i,j=1\\ i\neq j}}^{N}\left(\sum_{n=1}^{3} m_{ni}\cdot\vec{s}_{ni}\right)D_{ij}\left(\sum_{n=1}^{3} m_{nj}\cdot\vec{s}_{nj}\right) - \frac{1}{2}J_{\rm inter}\sum_{\langle i,j\rangle}[(\vec{s}_{2i}\cdot\vec{s}_{3j}) + (\vec{s}_{3i}\cdot\vec{s}_{2j})] - \sum_{i=1}^{N}\sum_{n=1}^{3} H m_{ni}(\vec{s}_{ni}\cdot\hat{e}_h). \quad (1)$$

The first, second, and third energy terms describe the nearest-neighbor Heisenberg exchange interaction between the core spin and the two surface spins, and the exchange interaction between the surface spins, respectively. The fourth and the fifth terms give the anisotropy energy for the core and the surface ($\hat{e}_i$ being the anisotropy easy-axis direction). The sixth term gives the dipolar interactions among all spins in the nanoparticles, where D_{ij} is the dipolar interaction tensor [22]. The next term describes the interparticle exchange interactions where $\langle i,j\rangle$ denotes summation over nearest neighbors. The last term is the Zeeman energy ($\hat{e}_h$ being the direction of the magnetic field). The parameters entering Eq. (1) are as follows:

(a) J_{c1}, J_{c2} are the intraparticle exchange coupling constants between the core spin and the surface spins and $J_{\rm srf}$ the exchange-coupling constant between the surface spins,

(b) $g = (M_s V)^2/4\pi d^3(20K_c V_1) \sim 3$ is the dipolar energy strength (where d is the smallest distance between two nanoparticles equal to the particle's diameter $d = 2$ nm), $M_S = 5.6 \times 10^2$ emu/cm^3, $K = 3 \times 10^4$ erg/cm^3 are the bulk values of saturation magnetization and the bulk anisotropy constant of the $MnFe_2O_4$ ferrite, respectively [25]. The saturation magnetization ratios have been extracted from atomic-scale calculations [26] for the spinel structure of a 2-nm-diameter

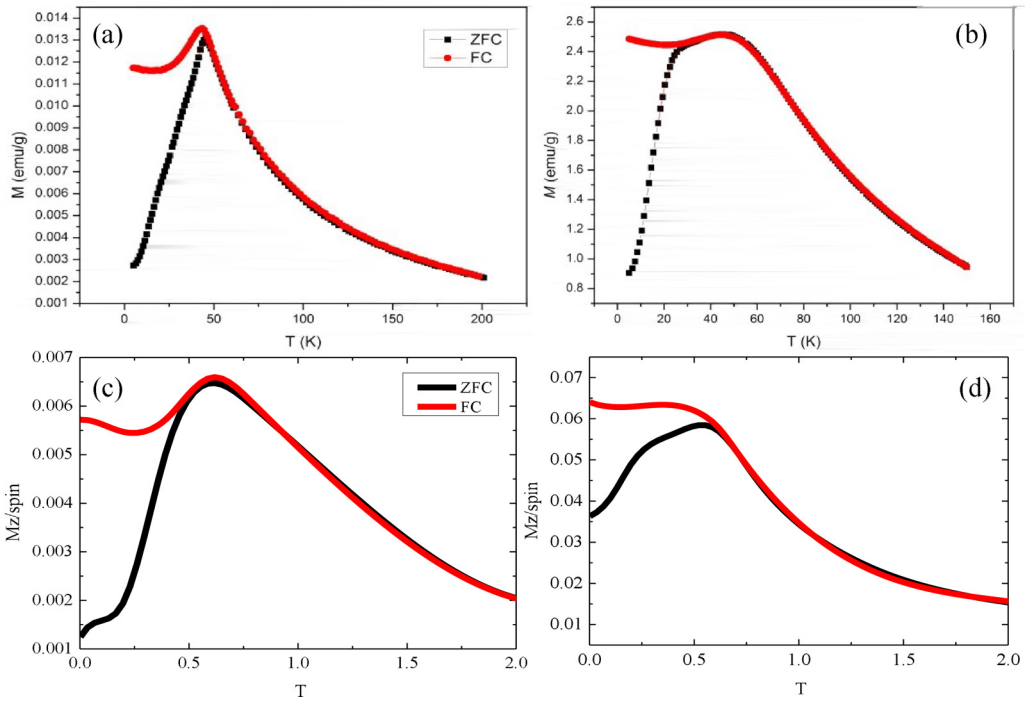

FIG. 2. Experimental data (upper panel) and Monte Carlo simulations (lower panel) of the ZFC-FC magnetization curves at a low (a), (c) and a high (b), (d) applied field.

$MnFe_2O_4$ nanoparticle, assuming 0.5-nm surface thickness, and they are $m_1 = 0.1, m_2 = 0.5, m_3 = 0.4$.

(c) the interparticle exchange coupling constant J_{inter},

(d) the anisotropy constant of the core K_C and of the surface K_{srf}, and

(e) the external magnetic field is H. The thermal energy is $k_B T$ (where T is the temperature).

The above energy parameters, as they are inserted in the simulations, have been normalized by the factor $20 \times K_C\, V_1$, where V_1 is the core volume of the nanoparticle, so they are dimensionless.

These parameters in Eq. (1) are based on the bulk values of $MnFe_2O_4$ and their modifications for the exchange-coupling constants and the surface anisotropy are established considering the nanoparticles' morphology (e.g., reduced symmetry and reduced size) using atomic-scale calculations and a mean-field approach [24]. Accordingly, the values of the intraparticle effective exchange-coupling constants among the core spin and the surface spins are $j_{c1} = 0.5$, $j_{c2} = 0.45$, $j_{\text{srf}} = -1.0$. The effective anisotropy constants for the core is $k_C = 0.05$ and for the surface is $k_{\text{srf}} = 1.0$. The strong random surface anisotropy combined with the intraparticle exchange coupling between the three spins creates internal frustration.

The interparticle exchange interaction between the surface spins of neighboring particles is taken as antiferromagnetic. There is not an exact microscopic model for the calculation of the exchange-coupling constants between the nanoparticles. So, we treat them as free parameters. We take the interparticle exchange-coupling constant $j_{\text{inter}} = -0.50$ half of the exchange coupling constant of the surface, since only a fraction of the shell comes into contact with the neighbouring shells. The magnetic configuration was obtained by a Monte Carlo simulation, using the standard Metropolis algorithm [27]. For the dipolar energy calculation the Ewald summation technique [22] has been implemented taking into account the long-range character of the dipolar interactions, using periodic boundaries in all directions.

The Monte Carlo simulations results for a given temperature and applied field were averaged over 80 samples with various spin configurations, realizations of the easy-axes distribution, and different spatial configurations for the nanoparticles. For the calculation of the zero-field-cooled (ZFC) curves the steps described below were followed: (1) Cooling the system at a constant step rate $\Delta T = 0.02$ every 5500 Monte Carlo (MC) steps from temperature $T = 2$ to $T = 0.002$ at zero applied field $H = 0$; (2) heating the sample from temperature $T = 0.002$ to $T = 2$ at the same constant step rate under the application of a magnetic field H_{app} and we calculate the ZFC curve; and (3) by field cooling (FC) down to $T = 0.002$ we calculate the FC curve. The hysteresis is calculated under a field-cooling procedure with a cooling field $H_{\text{cool}} = 2.5$ along the z direction. For every field and temperature value, the first 500 steps per spin are used for equilibration, and the subsequent 5000 MC steps are used to obtain thermal averages.

III. RESULTS AND DISCUSSION

In Fig. 2 (upper panel) we show the experimental ZFC/FC magnetization vs T (reduced units) curves for the $MnFe_2O_4$ nanopowders, synthesized by coprecipitation of Fe^{3+} and Mn^{2+} from water-in-toluene reverse-micelle system and subsequent thermal treatment at 320 °C, for applied field $H_{\text{app}} =$ 10 Oe (a) and $H_{\text{app}} = 3000$ Oe (b). The low-field experimental curves show a sharp maximum in both the ZFC and FC magnetization, the latter being weakly temperature dependent at lower temperature. This behavior is typical of a SSG system

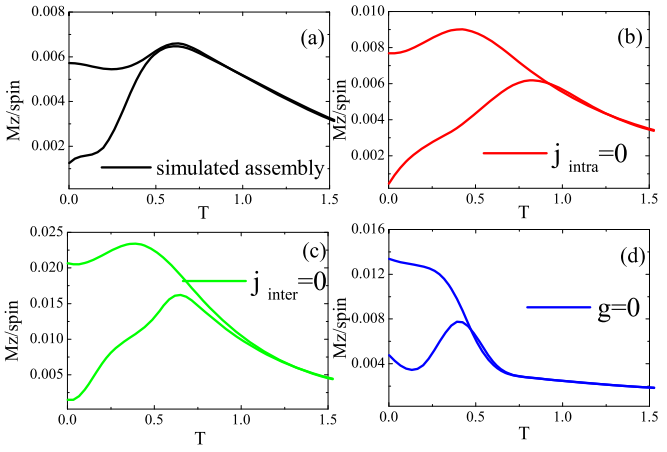

FIG. 3. Monte Carlo simulations of the ZFC magnetization curves for applied field $H_{\rm app} = 0.03$ for the simulated system (a); without including intraparticle characteristics ($j_{\rm inter} = 0$) (b); without including exchange-interparticle interactions ($j_{\rm inter} = 0$) (c); and without including dipolar interparticle interactions ($g = 0$) (d).

[12], resulting from the coexistence of disorder and frustration due to the presence of competing effects. The peak corresponds to the freezing temperature T_f of the SSG system. In the lower panel are presented the corresponding simulated curves for a low $H_{\rm app} = 0.03$ (c) and a high $H_{\rm app} = 0.2$ (d) applied field. Importantly, the parameters of the model reproduce quite well the SSG experimental findings, including the tendency to an increase of the FC magnetization at very low temperature.

In order to investigate the role of the intraparticle interactions, and the interparticle (dipolar and exchange) interactions on the SSG, simulations were also performed for the ZFC/FC magnetization curves by removing from the Hamiltonian: (1) the intraparticle interactions ($j_{\rm inter} = 0$, that is $j_{c1} = 0.0$, $j_{c2} = 0.0$, $j_{\rm srf} = 0.0$), (2) the exchange interparticle term ($j_{\rm inter} = 0$), and (3) the interparticle dipolar interactions ($g = 0$). In Fig. 3 the Monte Carlo simulations for all these cases of ZFC/FC magnetization curves, under a low applied field $H_{\rm app} = 0.03$, are presented together with simulations of the studied system for comparison [Fig. 3(a)].

The results of the simulations show that all types of interactions have to be taken into account to reproduce satisfactorily the experimental findings. Both in Fig. 3(b) (absence of intraparticle interactions) and in Fig. 3(c) (absence of exchange interparticle interactions) the maximum of the FC magnetization is shifted to lower temperature with respect to that of the ZFC one. The biggest deviation from the experimental curve is observed in Fig. 3(d) (absence of dipolar interactions), where the FC magnetization does not show a maximum. This behavior provides the confirmation that, although all the above terms contribute to stabilize the collective disordered frozen state, dipolar interactions play the dominant role due to their nondirectional character. The fact that the FC magnetization continues to increase with decreasing temperature and that the maximum of the ZFC one shifts to lower temperature reveals that in the absence of dipolar interactions the system moves from a collective SSG freezing to a blocking process of weakly interacting particles.

In the upper panel of Fig. 4 we show the Monte Carlo simulation results for the temperature dependence of the coercive (H_C) and the exchange-bias (H_{ex}) fields (a) together with the hysteresis loops at temperature $T = 0.01$ (b), under a

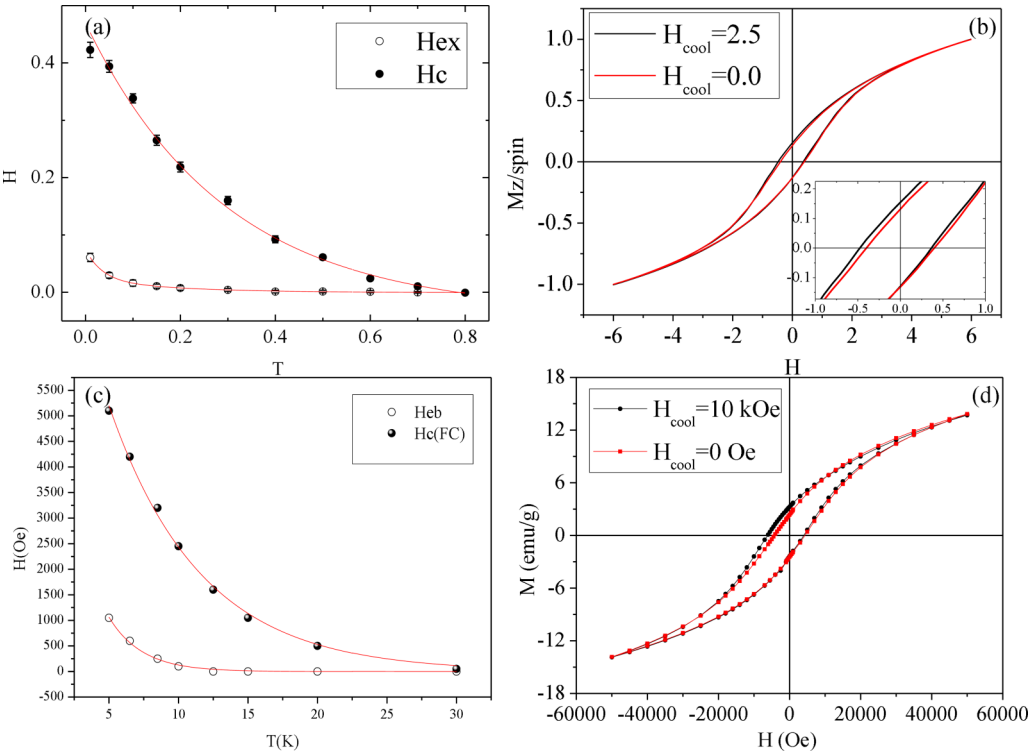

FIG. 4. Monte Carlo simulations (a), (b) and experimental data (c), (d) for the temperature dependence of H_C and H_{ex} (a), (c) and the hysteresis loops (b), (d) after a field-cooling procedure (black line). The hysteresis loops after a cooling procedure without any applied field are also presented (red line) at $T = 0.01$ (simulations) and $T = 5$ K (experiments).

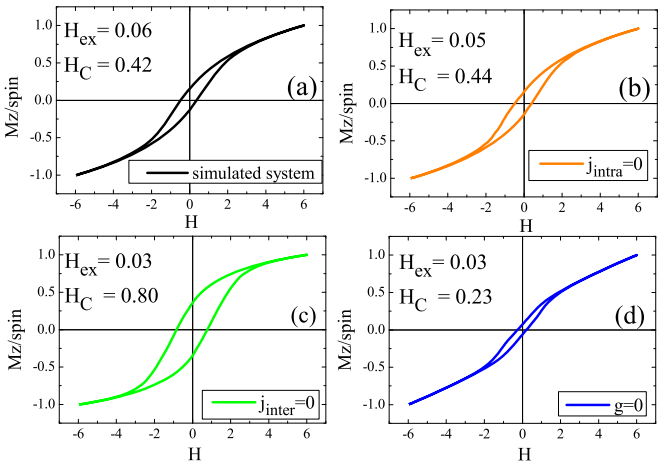

FIG. 5. Monte Carlo simulations of the hysteresis loops after a field-cooling procedure for the simulated system (a); for the case that we do not include (b) intraparticle interactions ($j_{\text{inter}} = 0$); (c) exchange-interparticle ($j_{\text{inter}} = 0$) and (d) interparticle dipolar interactions, at temperature $T = 0.01$.

cooling field $H_{\text{cool}} = 2.5$ (black line) and without any applied field (red line). Figures 4(c) and 4(d) show the corresponding experimental results for the $MnFe_2O_4$ nanopowders.

The simulated curves reproduce well the experimental ones. The hysteresis loops do not saturate as in the experimental hysteresis cycles which are measured up to 5 T. The exchange-bias field (H_{ex}) is seven times lower than the coercive field, close to the experimental case. Starting below the temperature at which the system becomes superparamagnetic, H_C increases exponentially with decreasing temperature, whereas H_{ex} appears at a much lower temperature, close to the beginning of the flattening of the FC magnetization with decreasing temperature, which indicates a complete freezing of the magnetic system, including the disordered surface spins. This indicates that the observed exchange-bias behavior in our dense assembly of magnetic particles is closely related to the freezing process and is the result of the interplay of intraparticle and interparticle interactions effects.

We have also calculated the low-temperature hysteresis loops after a field-cooling procedure with a cooling field $H = 2.5$ in the case that we do not take into account (1) the intraparticle interactions ($j_{\text{inter}} = 0$), (2) the exchange interparticle interactions ($j_{\text{inter}} = 0$), and (3) the dipolar interparticle interactions ($g = 0$) together with the simulated assembly for comparison. In Fig. 5 we present the MC simulation results for the above cases. The hysteresis loops are normalized to the saturation magnetization at the reference field value $H = 6$.

Figure 5(a) reports the simulated cycle including all the parameters of our model. In Fig. 5(b), where the intraparticle interactions are absent, the system has an exchange-bias field, which is due to the coupling between surface spins of the exchange-coupled neighboring nanoparticles, inducing an extra unidirectional anisotropy which competes with the random anisotropy of the surface and causes also an increase of the H_C. We must note that in this case the neighboring atoms being in contact give a thicker surface layer and enhanced volume anisotropy. Therefore, the exchange coupling between surface spins of particles in contact should contribute significantly to the exchange-bias effects. However, H_{ex} is 20% reduced with the value for the simulated system indicating that there are other contributions to H_{ex}. In Figs. 5(c) and 5(d), where exchange interparticle interactions and dipolar interactions are absent, respectively, H_{ex} is further decreased (50%), showing that the exchange-bias effect is strongly affected by interparticle interactions and it is closely related to the SSG freezing. In the absence of exchange-interparticle interactions [Fig. 5(c)], the exchange bias mainly comes from the particle core/surface interface, but it should be masked by the strong surface disorder. This disorder together with the strong dipolar interactions results in a big increase of H_C. Finally, in Fig. 5(d), where the dipolar interactions are absent, the exchange-bias field is due to the intraparticle morphology (core/shell interface) and to the exchange between surface spins of the exchange-coupled neighboring nanoparticles.

IV. CONCLUSIONS

The magnetic behavior of dense assemblies of ultrasmall $MnFe_2O_4$ nanoparticles with an average size of ~2 nm has been studied with the employment of a mesoscopic model that includes three macrospins for the description of each nanoparticle, taking into account in this way the surface effects in each nanoparticle. Our model, which also includes the dipolar and exchange-interparticle interactions in the dense assembly, describes well the observed magnetic behavior of a $MnFe_2O_4$ powder. The MC simulations reproduce satisfactorily the FC/ZFC magnetization vs T curves, providing evidence of a superspin glass behavior, and the temperature dependence of the H_C and H_{ex}. This indicates that both the SSG behavior and the exchange-bias phenomenon come from the interplay of intraparticle and interparticle interactions effects. The simulations indicate that the main contribution to the exchange-bias effect comes from the intra- and interparticle exchange interactions, the role of the dipolar interactions being very important in the creation of the SSG phase.

[1] S. Hazra and N. N. Ghosh, J. Nanosci. Nanotechnol. **14**, 1983 (2014).

[2] K. K. Kefeni, T. A. M. Msagati, and B. B. Mamba, Mater. Sci. Eng., B **215**, 37 (2017).

[3] B. Cruz-Franco, T. Gaudisson, S. Ammar, A. M. Bolarín-Miró, F. S. De Jesús, F. Mazaleyrat, S. Nowak, G. Vázquez-Victorio, R. Ortega-Zempoalteca, and R. Valenzuela, IEEE Trans. Magn. **50**, 6798060 (2014).

[4] P. Trataj, M. del P. Morales, S. Veintemillas-Verdaguer, T. Gonzles-Carreo, and C. J. Serna, J. Phys. D **36**, R182 (2003).

[5] R. H. Kodama, A. E. Berkowitz, E. J. McNiff, Jr., and S. Foner, Phys. Rev. Lett. **77**, 394 (1996).

[6] R. Aquino, J. Depeyrot, M. H. Sousa, F. A. Tourinho, E. Dubois, and R. Perzynski, Phys. Rev. B **72**, 184435 (2005).

[7] D. Peddis, C. Cannas, G. Piccaluga, E. Agostinelli, and D. Fiorani, Nanotechnology **21**, 125705 (2010).
[8] K. N. Trohidou, M. Vasilakaki, D. Peddis, and D. Fiorani, IEEE Trans. Magn. **48**, 1305 (2012).
[9] C. R. Alves, R. Aquino, J. Depeyrot, F. A. Tourinho, E. Dubois, and R. Perzynski, J. Mater. Sci. **42**, 2297 (2007).
[10] *Magnetic Nanoparticle Assemblies*, edited by K. Trohidou (Pan Stanford Publishing, Singapore, 2014), p. 306.
[11] G. Margaris, M. Vasilakaki, D. Peddis, K. N. Trohidou, S. Laureti, C. Binns, E. Agostinelli, D. Rinaldi, R. Mathieu, and D. Fiorani, Nanotechnology **28**, 035701 (2017).
[12] M. S. Andersson, R. Mathieu, S. S. Lee, P. S. Normile, G. Singh, P. Nordblad, and J. A. De Toro, Nanotechnology **26**, 475703 (2015).
[13] E. Tronc, A. Ezzir, R. Cherkaoui, C. ChaneHac, M. Nogues, H. Kachkachi, D. Fiorani, A. M. Testa, J. M. Greneche, and J. P. Jolivet, J. Magn. Magn. Mater. **221**, 63 (2000).
[14] D. Peddis, F. Orruù, A. Ardu, C. Cannas, A. Musinu, and G. Piccaluga, Chem. Mater. **24**, 1062 (2012).
[15] G. Muscas, G. Singh, W. R. Glomm, R. Mathieu, P. A. Kumar, G. Concas, E. Agostinelli, and D. Peddis, Chem. Mater. **27**, 1982 (2015).
[16] A. Kostopoulou, K. Brintakis, M. Vasilakaki, K. N. Trohidou, A. P. Douvalis, A. Lascialfari, L. Mannaf, and A. Lappas, Nanoscale **6**, 3764 (2014).
[17] C. R. Vestal, Q. Song, and Z. J. Zhang, J. Phys. Chem. B **108**, 18222 (2004).
[18] B. Aslibeiki, P. Kameli, and H. Salamati, J. Appl. Phys. **119**, 063901 (2016).
[19] R. Gao, Y. Zhang, W. Yu, R. Xiong, and J. Shi, J. Magn. Magn. Mater. **324**, 2534 (2012).
[20] D. Fiorani and D. Peddis, J. Phys.: Conf. Ser. **521**, 012006 (2014).
[21] D. Peddis, M. Vasilakaki, K. N. Trohidou, and D. Fiorani, IEEE Trans. Magn. **50**, 2303304 (2014).
[22] G. Margaris, K. N. Trohidou, and J. Nogués, Adv. Mater. **24**, 4331 (2012).
[23] M. Bellusci, S. Canepari, G. Ennas, A. La Barbera, F. Padella, A. Santini, A. Scano, L. Seralessandri, and F. Varsano, J. Am. Ceram. Soc. **90**, 3977 (2007).
[24] See Supplemental Material at http://link.aps.org/supplemental/10.1103/PhysRevB.97.094413 for Mössbauer spectra analysis and mesoscopic model parameters.
[25] B. D. Cullity and C. D. Graham, *Introduction to Magnetic Materials* (Wiley-IEEE, Hoboken, New Jersey, 2009), p. 568.
[26] E. Eftaxias, M. Vasilakaki, and K. N. Trohidou, Mod. Phys. Lett. B **21**, 1169 (2007).
[27] K. Binder and D. W. Heermann, *Monte Carlo Simulation in Statistical Physics, An Introduction*, Vol. 80, Solid-State Sciences (Springer-Verlag, Berlin, 1988).